Korean J. Chem. Eng., 33(9), 2703-2710 (2016)
DOI: 10.1007/s11814-016-0152-0

pISSN: 0256-1115
eISSN: 1975-7220

Hydrochar preparation from black liquor by CO_2 assisted hydrothermal treatment: Optimization of its performance for Pb^{2+} removal

Yong Sun*,,†, Jing Ping Zhang**, Fei Guo***, and Lian Zhang****

*School of Engineering, Edith Cowan University, 270 Joondalup Drive Joondalup, WA 6027, Australia
**National Engineering Laboratory of Cleaner Production Technology, Institute of Process Engineering, Chinese Academy of Sciences, Beijing 100190, China
***Department of Sports Science and Technology, Shanxi Normal University, Xi'an 710068, China
****Department of Chemical Engineering, Monash University, VIC, 3800, Australia
(*Received 18 October 2015 • accepted 8 June 2016*)

Abstract−Hydrochar was produced from hydrothermal treatment of corn straw black liquor. Response surface methodology (RSM) and the central composite design (CCD) were employed for determination of optimal char with maximum Pb^{2+} removal capacity. The operational parameters such as hydrothermal temperature (°C), duration (min) and solid liquid ratio (LSR) were chosen as independent variables in CCD. The statistical analysis indicates that the effects of hydrothermal temperature, duration, LSR and combined effect of hydrothermal temperature and duration are all significant for the Pb^{2+} removal capacity. The optimal condition for achieving the maximum Pb^{2+} adsorption capacity is obtained as the following: hydrothermal temperature (205 °C), duration (28 min), LSR (12) with Pb^{2+} removal capacity reaching 47 mg/g. The BET specific surface area of char prepared at optimal conditions could reach 85 m^2/g.

Keywords: Hydrochar, Black Liquor, Hydrothermal, Pb^2, CCD

INTRODUCTION

Heavy metals contamination in drinking water poses one of major potential threats to the environment [1,2]. Cost-effective removal of heavy metals such as lead [3], chromium [4,5], and cadmium [6] from aqueous solution has attracted much attention due to more and more stringent environmental regulations [7-10]. Among current available technologies, separation technology by adsorption such as using porous carbonaceous adsorbents [11,12] is one of the best candidates for heavy metal removal from water solution due to its availability on large scale, cost-effectiveness and technical reliability [13-15]. For adsorption technology, preparation of adsorbents in a cost-effective and economical manner is pivotal to the process optimization and reactor sizing [16,17]. Broadly speaking, the thermal pyrolysis and hydrothermal approaches are the most widely adopted approaches for preparation of porous carbonaceous adsorbents [18-20]. Due to advantages of insensitivity to toxic or inhibiting substances, directly treating wet organic substrates, flexible application of solid fraction, and relatively less environmental impact [21,22], hydrothermal carbonization has drawn continuous attention in processing wet organic substances. In our recent works, we developed an improved system for cost-effective and less energy-intensive approach for preparation of hydrochar from non-wood black liquor [23]. It was found that the separation process was efficiently intensified [24], which significantly reduces demand of evaporation and downstream wastewater treatment. Optimization of the hydrochar preparation from corn stover BL using this CO_2 assisted hydrothermal carbonization, to the best of our knowledge, has never been published before. In this work, central composite design (CCD) statistical analysis was also employed to optimize the Pb^{2+} removal performance of the prepared char; the effects of hydrothermal temperature, reaction duration and liquid solid ratio (LSR) upon resultant char for lead removal using response surface methodology (RSM), the equilibrium and kinetic adsorption by resultant char prepared from optimal condition were closely investigated.

†To whom correspondence should be addressed.
E-mail: y.sun@ecu.edu.au, ysunipecas@gmail.com

EXPERIMENTAL SECTION

1. Preparation of Char

The moisture content of black liquor (BL) was evaporated to approximately 50% (weight basis). The elementary analysis of BL is shown in Table 1, and carbon content is relatively higher than other elements, indicating its good property for being used as carbonaceous precursor. The char was prepared by the following procedure: wet BL was dissolved into the deionized water with different LSR and then was hydrothermally treated at different temperatures with different durations. During hydrothermal reaction, the flue gas (CO_2) pressure was adjusted to be higher than the steam

Table 1. Elemental composition of BL

Element	Content (wt%)
C	46
H	5.4
N	0.6
O (Estimated by difference)	48

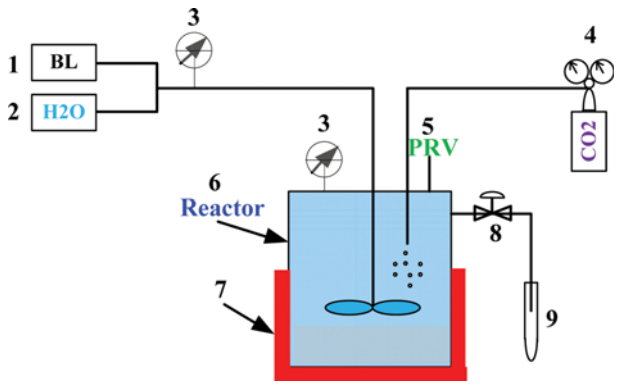

Fig. 1. Simplified schematic diagram of reaction system, where.

1. BL slurry tank
2. Dilution tank
3. Pressure gauge
4. CO_2 regulator
5. Pressure release valve
6. Reactor
7. Heating jacket
8. Back pressure needle valve
9. Sample cylinder

pressure with maximum 1 bar difference so that flue gas could be pressurized into the reactor to accelerate hydrothermal precipitation. The detailed experimental setup is in Fig. 1. The denotation of char carbonized at different temperature, duration and LSR is set as the following patterns: C-p1-p2-p3, where p1 represents parameter of hydrothermal temperature, p2 represents parameter of hydrothermal, p3 represents the parameter of LSR. For example, the sample C-205-28-12 represents sample being prepared with BL being carbonized at 205 °C for 28 minutes with LSR being at 12 in reactor.

2. Equilibrium and Kinetic Adsorption of Pb^{2+}

The simulated Pb^{2+} solution was prepared by dissolving Pb^{2+} in water. The Pb^{2+} concentration was determined by ICP-OES (Perkin-Elmer Optimal DV7300) by standard sample preparation and calibration methodology [25,26]. The dosage of adsorbent was varied from 0.01 to 0.08 g in a 250 ml glass flask. In preliminary study, we found that a dosage over 0.5 g/L would be reaching an equilibrium between metal ions and active surface site of the char. The standard Pb^{2+} solution of 50 ml with concentration varying from 10 to 100 ppm was added to the 250 ml glass flask dosed with the hydrochar to perform batch adsorption test. Form preliminary tests, the maximum adsorption performance will be around pH 8, so the pH value was pre-adjusted to be around 8 prior adsorption tests to maintain good performance for heavy metal adsorption. The isotherm was conducted at different temperature with 1 hour for reaching equilibrium by initial concentration varying from 10 to 100 mg/L. In this work, pH was adjusted by HNO_3 and NH_4OH.

The amount of adsorption at time t, q_t (mg/g), was expressed in the following:

$$q_t = \frac{(C_0 - C_t)V}{W} \tag{1}$$

For adsorption isotherm, the adsorbed Pb^{2+} at equilibrium q_e (mg/g) can be calculated as the following:

$$q_e = \frac{(C_0 - C_e)V}{W} \tag{2}$$

For kinetic analysis of the uptake of Pb^{2+} by char, the widely used pseudo-first-order and pseudo-second-order equations [27] were employed as follows:

$$\frac{1}{q_t} = \left(\frac{k}{q_e}\right)\frac{1}{t} + \frac{1}{q_e} \tag{3}$$

$$\frac{t}{q_t} = \frac{1}{kq_e^2} + \frac{t}{q_e} \tag{4}$$

For equilibrium isotherm [28,29], the Langmuir and Freundlich equations were employed as follows:

$$\frac{1}{q_e} = \frac{1}{(K_L q_m)C_e} + \frac{1}{q_m} \tag{5}$$

$$\log q_e = \log K_F + \log C_e \tag{6}$$

After the isotherms were obtained, the thermodynamic parameters were calculated using the following equations [30,31]:

$$\ln k_e = \frac{\Delta S}{R} - \frac{\Delta H}{RT} \tag{7}$$

$$\Delta G = \Delta H - T\Delta S \tag{8}$$

In Eq. (7), by applying different equilibrium constants against its corresponding temperatures (298, 308, 318 K), the standard entropy ΔS and standard enthalpy ΔH can be obtained. By combining results of Eq. (7) into Eq. (8) together with the variation of temperature (298, 308, 318 K), we obtained the standard Gibbs free energy at different temperatures. The one-set of standard entropy ΔS and standard enthalpy ΔH within (298-318 K) range and standard entropy ΔG at each different temperatures are shown in Table 7.

3. Characterization of Hydrochar

The specific surface area and pore size distribution of char were determined by nitrogen gas adsorption at 77 K with saturation pressure being set at 106.65 kPa using Micromeritics ASAP 2020 automated gas sorption system. The char samples were degassed (10^{-6} Torr) overnight at 350 °C. The specific surface area was estimated using the Brunauer-Emmett-Teller (BET) approach [32] within the range of relative pressures from 0.05 to 0.3. The pore size distribution was analyzed by density functional theory (DFT) approach.

FT-IR Analysis: The (Tensor-27) infrared spectrometer was employed for characterization AC. Sample was prepared by mixing the 1 mg AC with 0.4 g of KBr in an agate.

SEM morphology: Surface morphology was examined using a JSM-7001F+INCA X-MAX Field emission electron microscope.

Elemental analysis: the chromatography method was employed to analyze sample by Flash EA 1112 (Thermo Scientific).

4. Experimental Design and Statistical Analysis

A central composite design (CCD) [33,34] with three independent variables was used to study the response pattern and to determine the optimum combination of hydrothermal temperature, hydrothermal duration, LSR to maximize Pb^{2+} removal. The design with three independent variables at five different levels (total 20 runs) was adopted to find offset, linear, quadratic and interaction terms using the following equation [35]:

$$Y = b_0 + \sum_{i=1}^{3} b_i X_i + \sum_{i=1}^{3} b_{ii} X_i^2 + \sum_{i<j,\, j=2}^{3} b_{ij} X_i X_j \tag{9}$$

Table 2. Range and levels of independent process variables used for CDD (central composite design)

Independent variables	Symbols	$-\beta$	−1	0	1	β
Temperature/°C	X_1	190	195	200	205	210
Duration/min	X_2	20	25	30	35	40
LSR/-	X_3	6	8	10	12	14

Table 3. Three factors CCD with experimental results of dependent variables

Runs	Code values			Experimental results mg/g
	X_1	X_2	X_3	
1	200	30	6	40
2	195	25	12	24
3	200	30	10	43
4	195	35	8	38
5	205	35	8	33
6	200	20	10	39
7	200	40	10	37
8	195	35	12	34
9	205	25	12	42
10	210	30	10	41
11	205	35	12	38
12	195	25	8	26
13	205	25	8	40
14	200	30	14	44
15	190	30	10	18
16	200	30	10	40
17	200	30	10	43
18	200	30	6	40
19	200	30	10	43
20	200	30	10	44

The range and levels of variables optimized are shown in Table 2. The statistical significance of regression terms was checked by analysis of variance, ANOVA.

RESULTS AND DISCUSSION

1. Statistical Analysis and Optimization of Preparation Conditions

The experimental results associated with interaction between each independent variable are shown in Table 3. The Pb^{2+} removal capacity was found to be between 18 to 44 mg/g, respectively. Table 4 gives the ANOVA results for respective responses. The higher Fischer's '*F-statistics*' value and lower '*P*' value (probability) indicate the high significance of the regression model [36,37]. It is found that the terms X_1, X_1X_2, X_1^2, X_2^2 are quite significant, while other terms have less significance for response. By applying multiple regression analysis to the experimental data, the following second degree polynomial is derived to represent relationship between Pb^{2+} removal and three independent process variables (hydrothermal temperature, hydrothermal duration, LSR) as the following:

Table 4. ANOVA analysis for Pb^{2+} removal with r^2 0.93, Adjust r^2 0.92, Predicted r^2 0.92, adequate precision 13

Source	DF	Sum of squares	Mean square	F-value	Prob>F
Model	9	867.59	96.39	9.84	0.0007
X_1	1	367.98	367.98	37.57	0.0001
X_2	1	3.04	3.04	0.31	0.5896
X_3	1.00	6.10	6.10	0.62	0.4482
X_1X_2	1.00	141.20	141.20	14.42	0.0035
X_1X_3	1.00	18.15	18.15	1.85	0.2033
X_2X_3	1.00	0.45	0.45	0.05	0.8341
X_1^2	1.00	307.18	307.18	31.37	0.0002
X_2^2	1.00	50.47	50.47	5.15	0.0466
X_3^2	1.00	3.06	3.06	0.31	0.5884
Residue	10.00	97.92	9.79		
Lack of fit	5.00	89.56	17.91	10.71	0.0105
Pure error	5.00	8.36	1.67		
Cor total	19.00	965.52			

$$Y=41.8+9.59X_1+0.87X_2+1.14X_3-16.8X_1X_2+6.02X_1X_3 +0.95X_2X_3-14.4X_1^2-5.83X_2^2-1.29X_3^2 \quad (10)$$

The Pb^{2+} removal was evaluated in terms of removal capacity through 3-D plots of responses as a function of two factors while keeping the third parameter at the optimal condition (Fig. 2). The response patterns of combination effect of different process parameters to Pb^{2+} removal present a slightly different trend, especially in the combination effect of X_1X_2. In Fig. 2(a), the combined effect of hydrothermal temperature and duration enhances Pb^{2+} removal capacity of the resultant hydrochar. However, the combination of too high hydrothermal temperature and long hydrothermal duration will lead to a decrease of the Pb^{2+} removal capacity. At low level of hydrothermal temperature and duration, the increased hydrothermal temperature and duration will facilitate the carbonization and aggregation of the char, which increases the chance of creating external surface among the aggregated char particles. This could explain the slight increase of specific surface area of hydrochar and subsequent increase of Pb^{2+} removal amount. On the other hand, a too high level of hydrothermal temperature and duration will lead to a further gasification of the char under the harsh conditions and collapse of the formed external surfaces, which will result in a loss of surface functional groups that have strong affinity to the Pb^{2+} ion and drop of specific surface area. These all contribute to the decrease of Pb^{2+} removal capacity. In terms of response patterns of the combination effects of X_1X_3 and X_2X_3 in Fig. 1(b) and 1(c), response surface plots show a maximum region, which the removal of Pb^{2+} neither increases nor decreases, which indicates the existence of the optimal condition for maximizing the Pb^{2+} removal. Among these combined effects, only the combined effect of X_1X_2 (P=0.0035) is found to be significant to the response pattern [38]. The standard square r^2 for the quadratic model is 0.93, which indicates over 93% of the variation in the response could be explained by the model. The obtained adjusted r^2 was close to the experimental r^2 and predicted r^2, indicating a good agreement be-

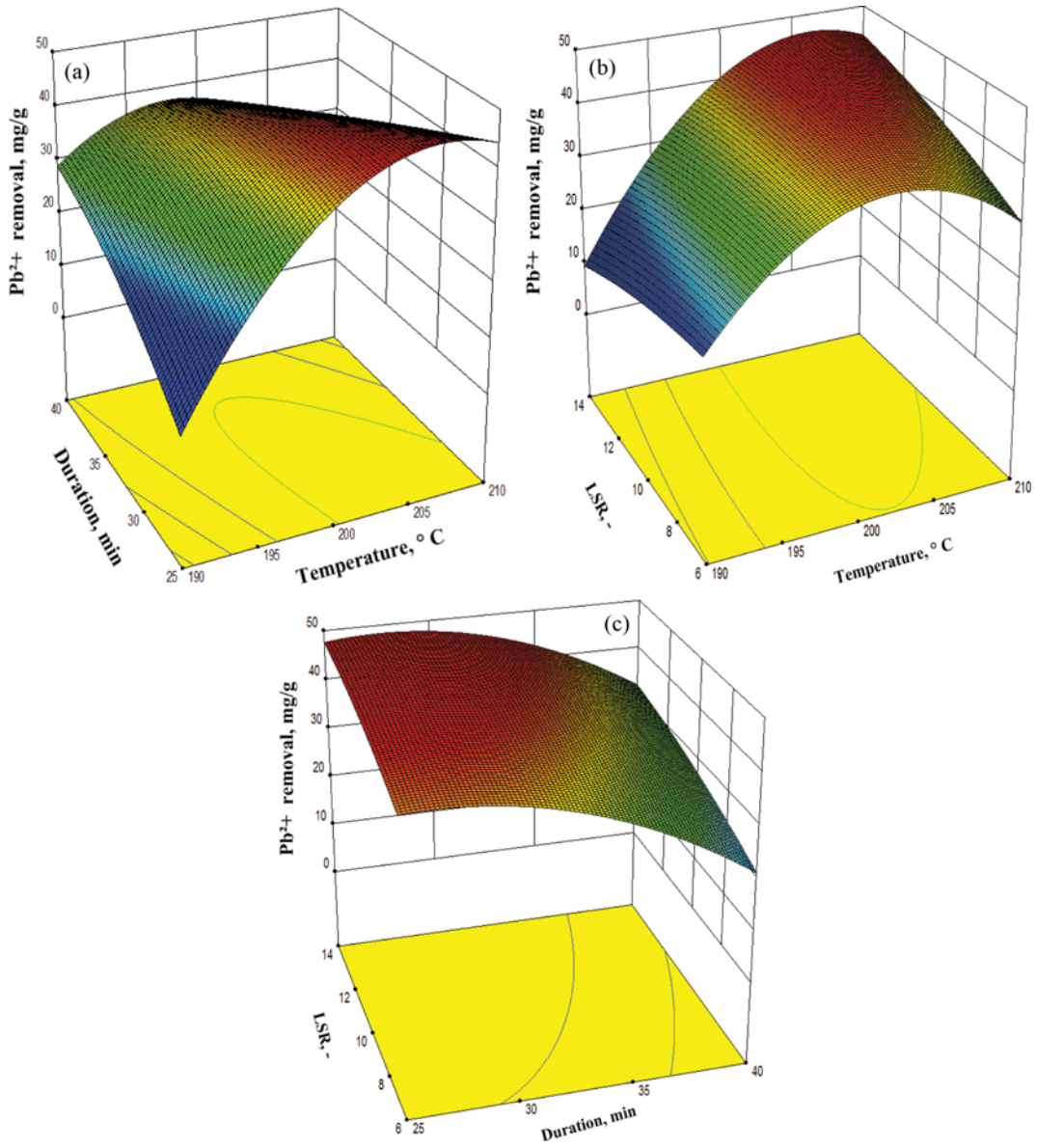

Fig. 2. Three-dimensional response surface for Pb^{2+} removal (a) hydrothermal temperature versus duration; (b) hydrothermal temperature versus LSR; (c) hydrothermal duration versus LSR.

tween experimental data and predicted values. The value of 'adequate precision' was 13.1, indicating an adequate signal.

Then the maximum Pb^{2+} removal capacity was set for optimization goal and 26 solutions were found. Out of them, the best condition selected was C-205-28-12, which represents that the sample was prepared with BL being carbonized at 205 °C for 28 min with LSR being at 12. The Pb^{2+} removal capacity predicted from the model could reach 45 mg/g. An experiment was also conducted to further validate the model prediction using equilibrium adsorption test, and the Pb^{2+} removal capacity of C-205-28-12 prepared at the optimal condition could reach 47 mg/g, indicating a 4.4% experimental deviation.

2. Effect of Hydrothermal Temperature and Char Characterization

Among those three independent parameters, the hydrothermal temperature was found to be the most significant (in form of single and combination effect) to the Pb^{2+} removal capacity. In this work, further investigations of the effects of hydrothermal temperature upon development of porosity of resultant hydrochar (keeping other process parameters at the optimal condition X_2=28 min and X_3=12) were conducted. The effect of hydrothermal temperature upon the BET specific surface area of hydrochar and their corresponding N_2 adsorption isotherms is shown in Fig. 3. The result indicates that the hydrothermal temperature increases the surface area when the activation temperature exceeds 190 °C, at which stage the specific surface area of C-205-28-12 reaches 85 m^2/g, while the BL without carbonization only presents a less than 10 m^2/g. In terms of nitrogen adsorption isotherms, the N_2 uptake of isotherms tends to take place at the entire pressure range, indicating the hydrothermal carbonization facilitates the creation of the external sur-

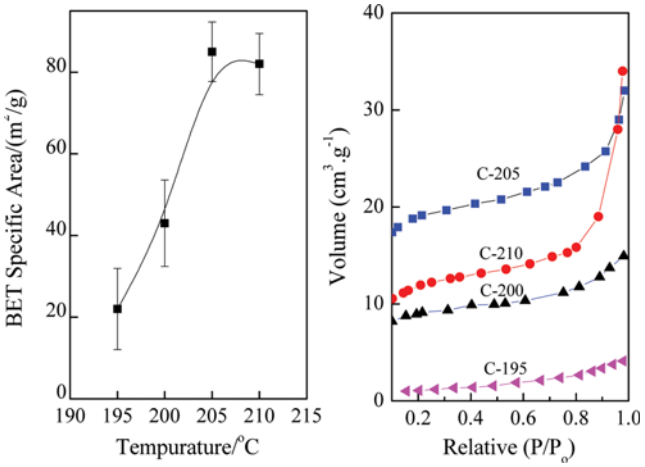

Fig. 3. Specific surface area as a function of activation temperature and N_2 adsorption isotherm of different chars with keeping duration and LSR as optimal conditions.

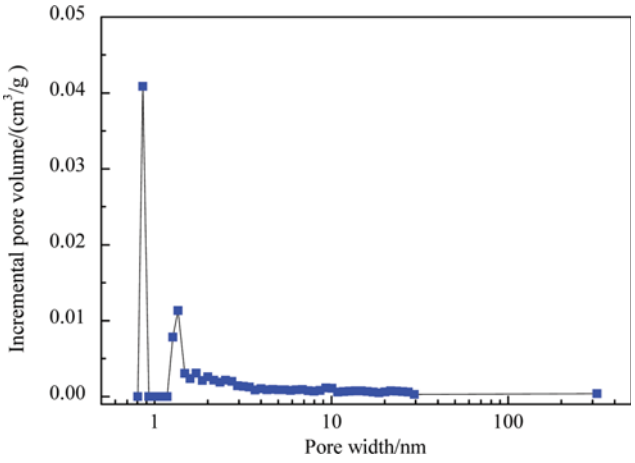

Fig. 4. DFT pore size distribution of prepared C-205 with keeping duration and LSR as optimal conditions.

face among the aggregated precipitated char. This leads to a slight increase of BET specific surface area. As hydrothermal temperature further increases being over 205 °C, a decrease of BET specific surface area of the resultant char is observed, indicating the harsh conditions destroy the created external surface among the aggregated chars. The DFT pore size distribution of C-205-28-12 is shown in Fig. 4. The prepared hydrochar possess a relatively wide pore size distribution that covers both micropore and mesopore region. The SEM morphology of BL and C-205-28-12 is shown in Fig. 5. Clearly, BL without hydrothermal treatment presents a completely different morphology to the hydrochar. SEM image of BL (Fig. 5(a)) shows the presence of lignocellulosic tissues and alkali crystals. The image from hydrochar (Fig. 5(b)) shows aggregated spherical microparticles, which come from decomposition of cellulose, hemicellulose and lignin compounds during hydrothermal carbonization. The aggregation of these microparticles will create external surface among these spherical particles; this result agrees with specific surface characterization. The FT-IR spectra of BL and C-205-

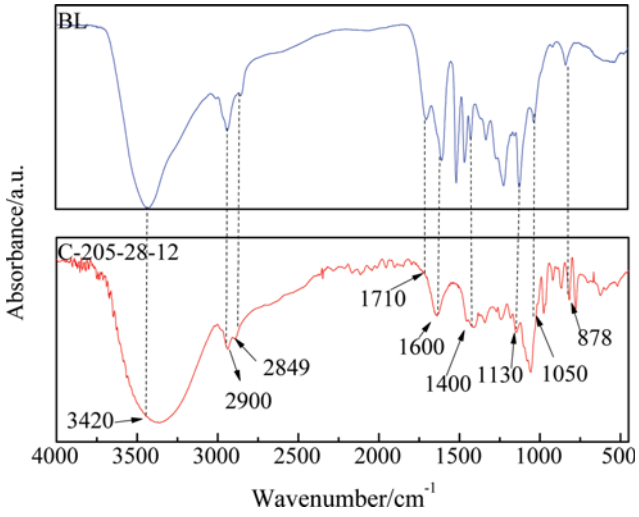

Fig. 5. FT-IR spectra of BL and C205-28-12.

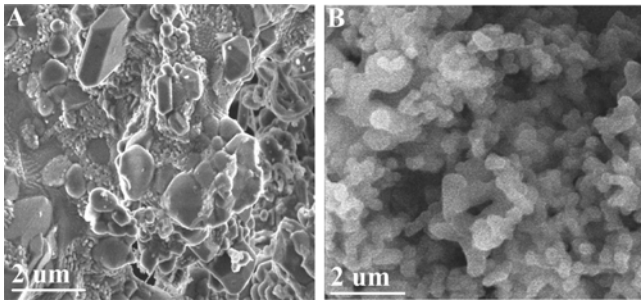

Fig. 6. SEM morphology of BL and C205-28-12.

28-12 are shown in Fig. 6. Before carbonization, the spectra of BL present characteristic bands of p-coumaryl, coniferyl, and sinapyl phenolic units, which center at 1,600, 1,510, 1,420 and 835 cm^{-1}, respectively [39]. When BL was carbonized, the intensity of those bands significantly decreased and even disappeared, indicating the intensive decomposition of phenolic compounds in BL matrix during carbonization. The band centered at 3,420 cm^{-1} is the characteristic band of OH group, indicating the adsorption of moisture [40]. When BL was carbonized, the intensity of this band also experienced a significant drop. The characteristic adsorption peaks of the valence vibration of CH groups [41] which center at 2,930, 2,849 and 1,120 cm^{-1}, the C-O stretching vibrations of carbonyl groups of which center at 1,130 cm^{-1}, and the C-O stretching of carbohydrate substance [42] of which the band centers at 1,050 cm^{-1} representing, all experience an significant decrease during activation, indicating the carbonization involving a complicated process, which includes dehydration, decomposition of aromatic compounds such as lignin and carbohydrates derived from cellulose and hemicellulose. It is also interesting that the intensity of the band, which represents the off-plane vibration of C=O groups [43] (band centers at 1,400 cm^{-1}) and valence vibration of C-O [44] (centers at 1,600 cm^{-1}) still remains quite obvious, indicating the existence of oxidative functional groups on the prepared hydrochar, and these remaining of surface functional groups will be beneficial for metal

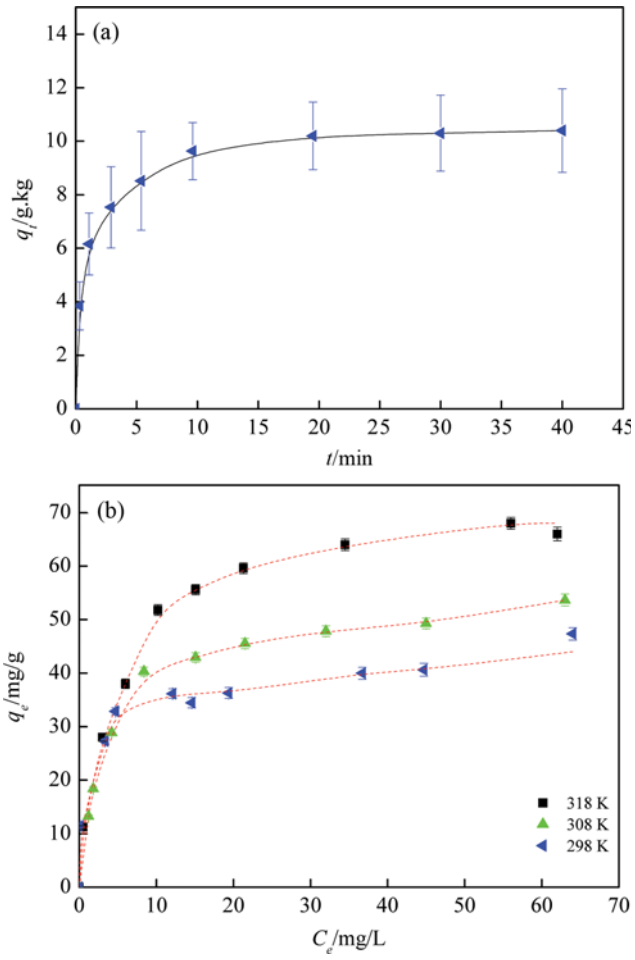

Fig. 7. Kinetics (a) and equilibrium (b) of C205-28-12 for Pb^{2+} adsorption.

Table 5. Kinetic constants of BL-850-2.1-38 using pseudo-first-order kinetics and pseudo-second-order kinetics

Model	q_{eq}/mg·g	k h^{-1}	q_e g·kg	r
Pseudo-first-order kinetics	8.5	1.2	9.1	0.90
Pseudo-second-order kinetics	8.5	0.09	8.7	0.99

ion adsorption.

3. Kinetic and Equilibrium Adsorption of Pb^{2+}

In this work, the adsorption kinetics is shown in Fig. 7(a). The corresponding kinetic constants are shown in Table 5. The pseudo-first-order and pseudo-second-order kinetics were employed to analyze kinetic adsorption. From r^2 value, the pseudo-second-order yields a better fit than the pseudo-first-order model. It indicates that the chemical bonding between divalent metal ions and polar functional groups on surface of the adsorbent plays a dominant role in determining the rate determining step [45].

The equilibrium isotherm and modeling constants of using Langmuir and Freundlich model are shown in Fig. 7(b) and Table 6. The Langmuir model presents a better fit than the Freundlich model for the isotherm curve modeling, and the corresponding calculated maximum monolayer loading of Pb^{2+} on adsorbent (q_m) could reach 45 mg/g. The estimation of Gibbs standard free energy, enthalpy and entropy were conducted and results are shown in Fig. 8 and Table 7. The negative value of Gibbs free energy indicates the spontaneous driving force of adsorption. The positive value of enthalpy indicates an endothermic process. Because of this thermodynamic property, the increased temperature creates a thermodynamically favorable condition for Pb^{2+} adsorption.

In Table 8, the Pb^{2+} adsorption capacity among different literature reports by different prepared adsorbents is compared. It is interesting that the Pb^{2+} adsorption capacity does not follow the order of porosity of the prepared adsorbent. This indicates that the adsorption of Pb^{2+} on the surface of adsorbent is more than a simple pore filling process; instead, much more complicated processes occur during adsorption. In terms of samples material, the Pb^{2+} adsorption capacity follows the order of Resin>Aginated-biochar>

Table 6. Langmuir and Freundlich model constants for Pb^{2+} on C205-28-12

Langmuir	Temperature/ K	K_L $L·mg^{-1}$	q_m mg·g	r^2
	298	0.47	45	0.95
	308	0.32	53	0.97
	318	0.24	60	0.91
Freundlich		n $L·mg^{-1}$	K_F mg·g	r^2
	298	4	16.1	0.94
	308	4.1	18.9	0.93
	318	4.1	24.5	0.90

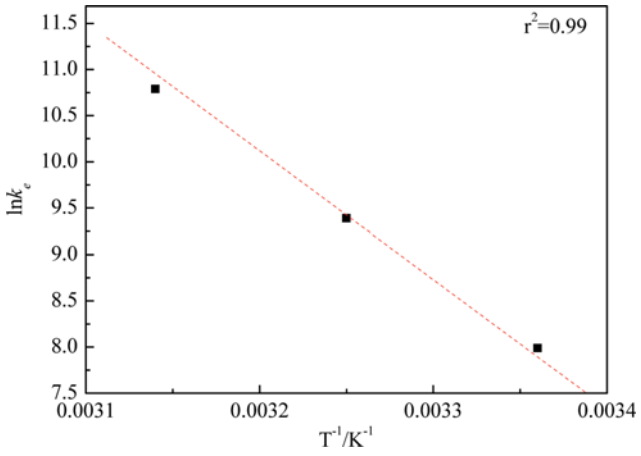

Fig. 8. Estimation of Gibbs standard free energy, enthalpy and entropy for removal of Pb^{2+} on C205-28-12.

Table 7. Thermodynamic constants for Pb^{2+} on C205-28-12

Temperature/ K	ΔG kJ·mol^{-1}	ΔH kJ·mol^{-1}	ΔS kJ·mol^{-1}
298	−1.8	10	42
308	−2.2		
318	−2.4		

Table 8. Comparison of Pb^{2+} adsorption capacity of different adsorbents prepared from different precursors and approaches

Sample	SSA m^2/g	Approach	Adsorption capacity mgg^{-1}	Reference
Organic waste	5	Hydro	6.8	[46]
Rice husk	-	Hydro	4.5	[47]
P. africana shell	10	Hydro	45	[48]
ZSM-5 zeolite	690	Hydro	120	[49]
Resin	-	Hydro	395	[50]
Charcoal	50	Pyrolysis	1.5	[51]
Char	23	Pyrolysis	1	[52]
Fly ash	20	Pyrolysis	2	[53]
Activated carbon	1322	Pyrolysis	43.5	[54]
Biochar-aginated	314	Pyrolysis	263	[55]
C-205-28-12	85	Hydro	47	This work

ZSM-5 zeolite>hydrochar (black liquor)>hydrochar (africana shell)> char (organic waste sulfonated)>fly ash>charcoal. Clearly, the introduction and modification of surface functional groups will enhance electrostatic interaction between the Pb^{2+} ion and surface of adsorbent. This could explain why the ion exchange resin and aginated biochar possess superior performance in Pb^{2+} removal than other adsorbents. The hydrochar prepared by the hydrothermal process also being rich with surface functional groups, which is confirmed from FTIR characterization in this work, is found to perform well in removal of metal ions as well. Considering the advantages of less environmental impact and direct processing wet organic precursor, the proposed process in this work is promising for large scale utilization of non-wood black liquor with relatively less environmental impact.

CONCLUSIONS

Hydrochar was produced from CO_2 assisted hydrothermal treatment from corn stover black liquor. The optimal condition was determined by using RSM with the operational parameters set as the following: activation temperature (205 °C), duration (28 mins), LSR (12) with Pb^{2+} removal capacity reaching 47 mg/g. The combination of hydrothermal temperature and duration was found to be significant to the response. The BET specific surface area of the hydrochar produced at optimal conditions could reach 85 m^2/g with the combination of micropores and mesopores. FTIR result indicates the presence of oxidative surface functional groups on the resultant hydrochar. The kinetic adsorption indicates a fast uptake of Pb^{2+}. The prepared hydrochar shows a comparable Pb^{2+} removal capacity at ambient temperature.

ACKNOWLEDGEMENTS

The National High Technology Research and Development Program 863 (2011AA060703) is highly appreciated for financial support. Anpeng high-tech energy and resource company is highly appreciated for supporting this work. Authors would like to give special thanks for fruitful discussions with Dr Yarong Li from NSW government of department of environmental protection for better improvement of this work. The critical comments from three anonymous reviewers are highly appreciated.

NOMENCLATURE

b_0 : intercept coefficient
b_i : linear coefficient
b_{ii} : quadratic coefficient
C_0 : initial concentration [mgL^{-1}]
C_e : equilibrium concentration [$mg\ L^{-1}$]
C_t : concentration at time of t [mgL^{-1}]
ΔG : Gibbs free energy [$kJ\ mol^{-1}$]
ΔH : adsorption enthalpy [$kJ\ mol^{-1}$]
k_e : kinetic constants [-]
K_F : Freundlich constants [Lmg^{-1}]
K_L : Langmuir constants [Lmg^{-1}]
q_e : equilibrium absorbed concentration [$g\ kg^{-1}$]
q_m : Langmuir monolayer saturation adsorption amount [$g\ kg^{-1}$]
q_t : absorbed concentration at time t [$g\ kg^{-1}$]
R : pressure gases constant [0.00831 $kJ\ mol^{-1}K^{-1}$]
ΔS : adsorption entropy [$kJ\ mol^{-1}$]
t : time [s]
T : temperature [K]
V : volume of phenol solution [L]
W : mass of adsorbent [kg]
X_i : independent variables [-]
Y : predicted response [%]
ANOVA : analysis of variance
CCD : central composite design
RSM : response surface methodology
LSR : liquid solid ratio [-]

REFERENCES

1. D. Pullini, V. Siong, D. Tamvakos, B. L. Ortega, M. F. Sgroi, A. Veca, C. Glanz, I. Kolaric and A. Pruna, *Compos. Sci. Technol.*, **112**, 16 (2015).
2. W. S. W. Ngah and M. A. K. M. Hanafiah, *Bioresour. Technol.*, **99**, 3935 (2008).
3. M. Ahmaruzzaman, *Adv. Colloid Interface Sci.*, **166**, 36 (2011).
4. Y. Sun, J. Wei, M. S. Yao and G. Yang, *Asia-Pac. J. Chem. Eng.*, **7**, 547 (2012).
5. Y. Sun, J. P. Zhang, G. Yang and Z. H. Li, *Environ. Technol.*, **28**, 491 (2007).
6. Y. V. Nancharaiah, S. V. Mohan and P. N. L. Lens, *Bioresour. Technol.*, **195**, 102 (2015).
7. V. Srivastava, P. K. Singh, C. H. Weng and Y. C. Sharma, *Pol. J. Chem. Technol.*, **13**, 1 (2011).
8. J. Singh, N. S. Mishra, Uma, S. Banerjee and Y. C. Sharma, *Bioresources*, **6**, 2732 (2011).
9. Y. X. Wang, H. H. Ngo and W. S. Guo, *Sci. Total Environ.*, **533**, 32 (2015).
10. M. Adibfar, T. Kaghazchi, N. Asasian and M. Soleimani, *Chem. Eng. Technol.*, **37**, 979 (2014).
11. S. H. Kwon, E. Lee, B. S. Kim, S. G. Kim, B. J. Lee, M. S. Kim and

J. C. Jung, *Korean J. Chem. Eng.*, **32**, 248 (2015).
12. S. S. A. Syed-Hassan and M. S. Md Zaini, *Korean J. Chem. Eng.* (2016), DOI:10.1007/s11814-016-0072-z.
13. Y. Sun, G. Yang, J. P. Zhang, Y. S. Wang and M. S. Yao, *Chem. Eng. Technol.*, **35**, 309 (2012).
14. X. F. Song, X. Y. Ji, H. P. Bie, Q. Q. Liu and R. S. Bie, *Fuel*, **159**, 89 (2015).
15. P. Hadi, M. Xu, C. Ning, C. S. K. Lin and G. McKay, *Chem. Eng. J.*, **260**, 895 (2015).
16. S. E. Moradi, *Korean J. Chem. Eng.*, **31**, 1651 (2014).
17. K. Mahmoudi, K. Hosni, N. Hamdi and E. Srasra, *Korean J. Chem. Eng.*, **32**, 274 (2015).
18. S. L. Zhang, L. C. Tao, M. Jiang, G. J. Gou and Z. W. Zhou, *Mater Lett.*, **157**, 281 (2015).
19. Y. Sun, J. Wei, Y. S. Wang, G. Yang and J. P. Zhang, *Environ. Technol.*, **31**, 53 (2010).
20. Y. Sun, J. P. Zhang, G. Yang and Z. H. Li, *Chem. Biochem. Eng. Q*, **21**, 169 (2007).
21. Y. Sun, G. Yang, C. Wen, L. Zhang and Y. S. Wang, *Environ. Prog. Sustain*, **33**, 581 (2014).
22. K. Tekin, S. Karagoz and S. Bektas, *Renew. Sust. Energy Rev.*, **40**, 673 (2014).
23. Y. Sun, J. P. Zhang, C. Wen and L. Zhang, *Chem. Eng. Process.: Process Intensification*, **104**, 1 (2016).
24. J. P. Zhang, Y. Sun, M. W. Woo, L. Zhang and K. Z. Xu, *J. Taiwan Inst. Chem. E*, **59**, 395 (2016).
25. Y. Sun, G. Yang, J. P. Zhang and Z. H. Li, *Spectrosc. Spect. Anal.*, **27**, 371 (2007).
26. Y. Sun, J. P. Zhang, G. Yang and Z. H. Li, *Spectrosc. Spect. Anal.*, **27**, 1424 (2007).
27. Y. S. Ho and G. McKay, *Process. Biochem.*, **34**, 451 (1999).
28. J. Hu, B. J. Li, L. Y. Huang, J. Zuo, W. Zhang, W. C. Ying and M. R. Matsumoto, *Environ. Prog. Sustain*, **32**, 512 (2013).
29. A. E. Ensuncho-Munoz and J. G. Carriazo, *Environ. Technol.*, **36**, 547 (2015).
30. M. A. Richard, P. Benard and R. Chahine, *Adsorption*, **15**, 53 (2009).
31. M. A. Richard, P. Benard and R. Chahine, *Adsorption*, **15**, 43 (2009).
32. N. V. Sych, S. I. Trofymenko, O. I. Poddubnaya, M. M. Tsyba, V. I. Sapsay, D. O. Klymchuk and A. M. Puziy, *Appl. Surf. Sci.*, **261**, 75 (2012).
33. Y. Sun, J. Wei, J. P. Zhang and G. Yang, *J. Natural Gas Sci. Eng.*, **28**, 173 (2016).
34. Y. Sun, J. P. Zhang and L. Zhang, *Environ. Prog. Sustain*, In Press (2016) DOI:10.1002/ep.12365.
35. N. Chaudhary and C. Balomajumder, *J. Taiwan Inst. Chem. E*, **45**, 852 (2014).
36. Y. Sun, G. Yang, Z. H. Jia, C. Wen and L. Zhang, *Chem. Ind. Chem. Eng. Q*, **20**, 531 (2014).
37. Y. Sun, J. P. Zhang, C. Wen and Z. H. Li, *J. Taiwan Inst. Chem. E* (2016), DOI:10.1016/j.jtice.2016.1002.1030.
38. Y. Sun, J. P. Zhang, G. Yang and Z. H. Li, *Environ. Prog.*, **26**, 78 (2007).
39. Y. Sun, J. P. Mang, G. Yang and Z. H. Li, *Spectrosc. Spect. Anal.*, **27**, 1997 (2007).
40. L. H. Huang, J. J. Kong, W. L. Wang, C. L. Zhang, S. F. Niu and B. Y. Gao, *Desalination*, **286**, 268 (2012).
41. C. H. Chia, B. Gong, S. D. Joseph, C. E. Marjo, P. Munroe and A. M. Rich, *Vib Spectrosc*, **62**, 248 (2012).
42. T. Chen, Z. Y. Zhou, R. Han, R. H. Meng, H. T. Wang and W. J. Lu, *Chemosphere*, **134**, 286 (2015).
43. B. X. Shen, J. H. Chen, S. J. Yue and G. L. Li, *Fuel*, **156**, 47 (2015).
44. G. L. Li, B. X. Shen, Y. W. Li, B. Zhao, F. M. Wang, C. He, Y. Y. Wang and M. Zhang, *J. Hazard. Mater*, **298**, 162 (2015).
45. Y. S. Ho, J. C. Y. Ng and G. Mckay, *Sep. Sci. Technol.*, **36**, 241 (2001).
46. N. C. Deborah Ruziwa, Willis Gwenzi, Innocent Pumure, *J. Environ. Chem. Eng.*, **3**, 2528 (2015).
47. Z. G. Liu and F. S. Zhang, *J. Hazard. Mater*, **167**, 933 (2009).
48. S. E. Elaigwu, V. Rocher, G. Kyriakou and G. M. Greenway, *J. Ind. Eng. Chem.*, **20**, 3467 (2014).
49. I. O. Ali, A. M. Hassan, S. M. Shaaban and K. S. Soliman, *Sep. Purif. Technol.*, **83**, 38 (2011).
50. H. Guo, Y. Z. Ren, X. L. Sun, Y. D. Xu, X. M. Li, T. C. Zhang, J. X. Kang and D. Q. Liu, *Appl. Surf. Sci.*, **283**, 660 (2013).
51. E. A. El-Sofany, W. F. Zaher and H. F. Aly, *J. Hazard. Mater*, **165**, 623 (2009).
52. M. Bernardo, S. Mendes, N. Lapa, M. Goncalves, B. Mendes, F. Pinto, H. Lopes and I. Fonseca, *J. Colloid Interface Sci.*, **409**, 158 (2013).
53. S. Mohan and R. Gandhimathi, *J. Hazard. Mater*, **169**, 351 (2009).
54. J. Acharya, J. N. Sahu, C. R. Mohanty and B. C. Meikap, *Chem. Eng. J.*, **149**, 249 (2009).
55. X. H. Do and B. K. Lee, *J. Environ. Manage.*, **131**, 375 (2013).